Pergamon

Int. J. Solids Structures Vol. 31, No. 23, pp. 3175–3199, 1994

0020–7683/94 $7.00 + .00

0020-7683(94)00096-4

THE EDGE CRACKING AND DECOHESION OF THIN FILMS

A. R. AKISANYA and N. A. FLECK
Cambridge University Engineering Department, Trumpington Street, Cambridge CB2 1PZ, U.K.

(*Received* 26 *January* 1994; *in revised form* 22 *May* 1994)

Abstract—The cracking and decohesion processes that may accompany a residually stressed thin film on a substrate have been investigated. Attention is focused on an interfacial edge crack, loaded by a linear variation of residual stress across the thickness of the film. The interfacial stress intensity factor and the non-singular T-stresses at the interfacial crack tip are evaluated using the finite element method, and the role of the T-stresses and the interfacial phase angle in influencing the selection of crack path is discussed. The results are used to predict the distributions of residual stress for which kinking switches from the substrate to the film.

1. INTRODUCTION

Decohesion of residually stressed thin films is of current concern because of the extensive use of these materials in integrated circuits, semiconductors and in magnetic disks. Residual stresses in thin films arise either from the deposition process (intrinsic stress), or from the difference in thermal expansion between the film and the substrate (thermal residual stress). In general, the residual stress is not uniform across the thickness of the film; a stress gradient exists in the film. For example, a stress difference between the inner and outer surfaces of the film, having the same order of magnitude as the mean stress in the film, has been reported for a chromium film on a glass substrate (Hu *et al.*, 1988).

In general, cracking and decohesion processes in film/substrate systems depend upon the sign and magnitude of the residual stress in the film, stress gradient in the film, relative elastic properties of the film and the substrate, and upon the relative fracture resistance of the film, substrate and of the film/substrate interface. Despite the recent progress in understanding the mechanics of failure in residually stressed thin film/substrate systems, the quantitative sensitivity of the initial stages of the decohesion process to the above parameters is mostly unknown.

Various cracking patterns in film/substrate systems have been observed and analysed (Hutchinson and Suo, 1992). The operative failure mode depends strongly upon the sign and distribution of the residual stress in the film. One important failure mode for film/substrate systems is the propagation of an interfacial crack from an edge defect, as shown in Fig. 1. Such decohesion may lead to the spalling of the film or to cracking within the substrate. Interfacial edge defects are often short and arise as a result of poor bonding between the film and the substrate during manufacture or as a result of physical damage to the film/substrate system.

1.1. *Statement of the problem*

In this paper we analyse, by the finite element method, the early stages of growth of an interfacial edge crack between a film of thickness h and a substrate of thickness H, as defined in Fig. 2(a). For computational simplicity we assume that a crack of length ℓ exists at each edge of the bimaterial of width $2L$ [see Fig. 2(a)]. The film is subjected to a tensile residual stress field which varies linearly with depth through the film from a value σ_2 at the top of the film to a value σ_1 at the bottom of the film. For the case $\ell \ll L$, the solution to the above problem coincides with that for a single edge crack of length ℓ, loaded by a linear distribution of normal traction at the edge of the film.

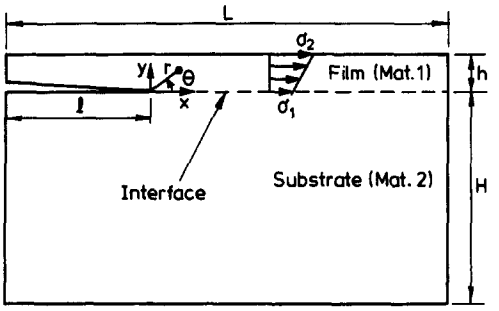

Fig. 1. An interfacial edge crack between a thin film and a substrate.

It is now shown by an Eshelby "cut and paste" procedure that the stress field in the cracked body due to a linear distribution of tensile residual stress in the film [Fig. 2(a)] is equivalent to the sum of:

(i) a linearly varying tensile stress in the film and a stress-free substrate [Fig. 2(b)];
(ii) the stress field in the cracked body due to a compressive normal traction at the edge of the film [Fig. 2(c)].

We start by assuming that the film and substrate are separated from each other (the "cut" operation) and the substrate is stress free. The film is assumed to be subjected to tensile "transformation stresses" σ_{xx} which vary linearly with depth, as shown in Fig. 2(b). These transformation stresses may be taken to arise from differential thermal contraction and from the deposition process itself ("intrinsic stresses"); imagine that the edges of the film

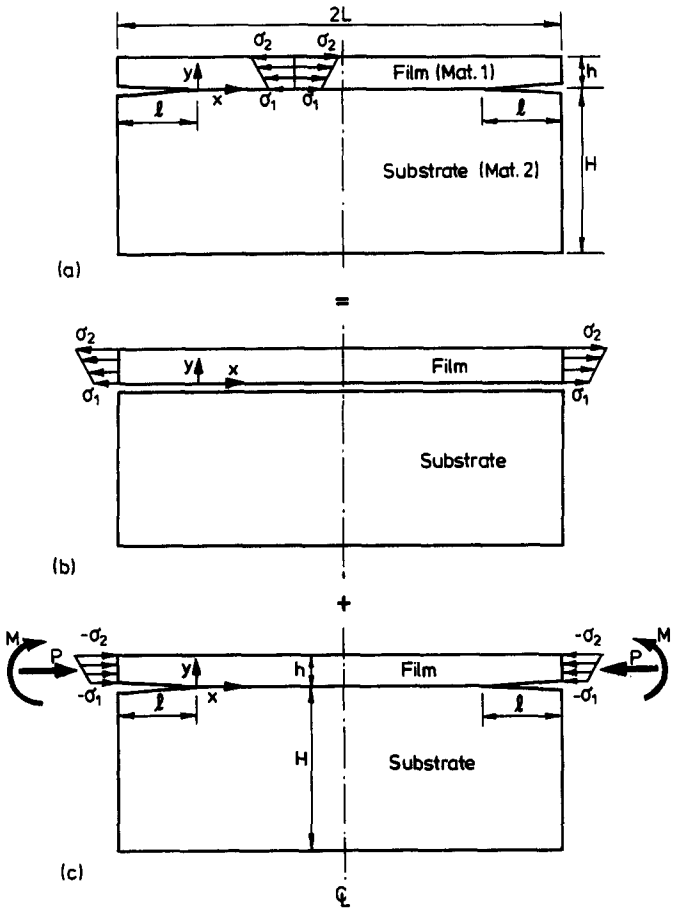

Fig. 2. The thin film/substrate geometry.

are pulled by external edge tractions in order to preserve the tensile stress distribution σ_{xx} in the film. Next, the film is placed on the substrate and bonded to it (the "paste" operation). The transformation stresses σ_{xx} at the edge of the film are then relaxed by applying compressive tractions $-\sigma_{xx}$ to the edge of the film. The change in stress due to this relaxation process is given by the solution to the problem of edge loading of the cracked bimaterial, as shown in Fig. 2(c). Finally, addition of the stress fields shown in Figs 2(b) and 2(c) gives the stress field in a cracked bimaterial due to a tensile residual stress field, as shown in Fig. 2(a). Note that the interfacial stress intensity factor at the tip of the cracks in Fig. 2(a) is the same as that shown in Fig. 2(c), since the loading in Fig. 2(b) does not give rise to a singular stress field. Finite element calculations are given later in the paper for the boundary value problem shown in Fig. 2(c). Results for the residual stress problem of Fig. 2(a) follow directly from the above superposition argument.

For the edge loading problem of Fig. 2(c), the interfacial stress intensity factor and the strain energy release rate are evaluated as a function of the interfacial crack length ℓ, stress gradient in the film, the relative film to substrate thickness, and the relative elastic properties of substrate and film. Implications for stable and unstable interfacial crack growth under fixed residual stress are discussed. The in-plane non-singular T-stress at the tip of the interfacial crack is calculated, and its role is evaluated in influencing kinking of an interfacial crack into the film or substrate.

2. REVIEW OF KINKING OF AN INTERFACIAL CRACK OUT OF THE INTERFACE

We shall examine whether kinking of an interfacial edge crack between a thin film and a substrate is expected. Before presenting the results we shall summarise the elastic theory of kinking of an interfacial crack, and the role played by the T-stress in influencing kinking. The theory draws heavily upon the work of He and Hutchinson (1989) and He *et al.* (1991).

Consider an interfacial plane strain crack between two isotropic elastic solids labelled 1 and 2, as shown in Fig. 1. Here we refer to the film as material 1 and to the substrate as material 2. The two elastic mismatch parameters of Dundurs (1969) which govern plane strain problems are

$$\alpha = \frac{\bar{E}_1 - \bar{E}_2}{\bar{E}_1 + \bar{E}_2} \tag{1a}$$

$$\beta = \frac{1}{2}\frac{(1-2\nu_2)/\mu_2 - (1-2\nu_1)/\mu_1}{(1-\nu_2)/\mu_2 + (1-\nu_1)/\mu_1}, \tag{1b}$$

where the subscripts refer to materials 1 and 2; E, μ and ν denote Young's modulus, shear modulus and Poisson's ratio, respectively. The overbar on the E designates the plane strain value, $\bar{E} = E/(1-\nu^2)$. The material parameter α is positive when the substrate (material 2) is more compliant than the film (material 1), and is negative when the substrate is stiffer than the film. Both α and β vanish when the elastic properties of the film and the substrate are identical. The (α, β) values for typical material combinations are concentrated along the $\beta = 0$ and $\beta = \alpha/4$ lines in α–β space (Suga *et al.*, 1988). Note that $\beta = \alpha/4$ corresponds to $\nu_1 = \nu_2 = \frac{1}{3}$. In the current paper we restrict our discussion to material combinations with $\beta = 0$ and $\beta = \alpha/4$.

In general, an interfacial crack between two dissimilar isotropic elastic solids suffers a singular stress field characterised by the complex interfacial stress intensity factor $K = K_1 + iK_2$, where $i \equiv \sqrt{-1}$. In order to define K we introduce the Cartesian co-ordinates (x, y) and polar co-ordinates (r, θ) as shown in Fig. 1. Then K is defined such that, at a distance r directly ahead of the crack tip, the normal stress σ_{yy} and shear stress σ_{xy} components are given by

$$\sigma_{yy} + i\sigma_{xy} = \frac{1}{\sqrt{2\pi}} K r^{-(1/2)+i\varepsilon} \tag{2}$$

where the oscillatory index ε depends only upon β via

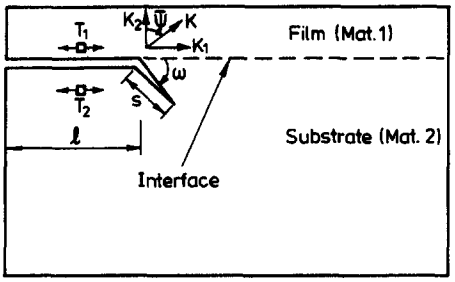

Fig. 3. Crack kinking out of the interface between a thin film and a substrate.

$$\varepsilon = \frac{1}{2\pi}\ln\left(\frac{1-\beta}{1+\beta}\right). \tag{3}$$

It is clear from eqn (2) that for $\varepsilon \neq 0$ the stress components oscillate as the crack tip is approached. This complicates the usual definition of mode mix at the crack tip. A rational approach suggested by Rice (1988) is to define the mode mix on the basis of the ratio σ_{xy}/σ_{yy} at a fixed distance $\hat{\ell}$ ahead of the crack tip. Accordingly, the phase angle $\hat{\psi}$ is introduced where

$$\tan\hat{\psi} = \left(\frac{\sigma_{xy}}{\sigma_{yy}}\right)_{r=\hat{\ell}} = \frac{\mathrm{Im}\,(K\hat{\ell}^{i\varepsilon})}{\mathrm{Re}\,(K\hat{\ell}^{i\varepsilon})}. \tag{4}$$

(For a homogeneous solid $\alpha = \beta = \varepsilon = 0$, and K_1 and K_2 can be interpreted as the classical mode I and II stress intensity factors, respectively.)

The energy release rate for advance of the interfacial crack G_I is

$$G_I = (K_1^2 + K_2^2)/E^*, \tag{5}$$

where $E^* \equiv (1+\alpha)/(1-\beta^2)\bar{E}_2$. For propagation of a crack along an interface the energy release rate G_I must attain the interfacial toughness Γ_I. In general Γ_I is observed to be a strong function of the phase angle $\hat{\psi}$. The length scale $\hat{\ell}$ chosen in the definition (4) of $\hat{\psi}$ is somewhat arbitrary. A physically sound strategy is to fix $\hat{\ell}$ at a characteristic "material length scale" ahead of the crack tip which controls the interfacial toughness; the idea is that the toughness Γ_I depends upon the ratio of shear stress σ_{xy} to normal stress σ_{yy} at some relevant distance $\hat{\ell}$ ahead of the crack tip. Thus Γ_I is a unique function of $\hat{\psi}$, where $\hat{\psi}$ is defined in eqn (4). As discussed by Rice (1988), the particular value taken for $\hat{\ell}$ usually has a negligible effect on the value of the phase angle $\hat{\psi}$ for realistic values of ε. Indeed for the case $\beta = \varepsilon = 0$, the phase angle $\hat{\psi}$ is independent of the particular choice of $\hat{\ell}$, as discussed by Hutchinson and Suo (1992).

The next higher order term in the series expansion of the crack tip stress field is given by in-plane direct stresses parallel to the crack plane, as sketched in Fig. 3. These stresses are of magnitude T_1 in material 1 and T_2 in material 2, and are referred to as the "T-stresses." Since the strain component ε_{xx} is the same on both sides of the interface, the T-stresses are in a fixed ratio given by

$$T_2 = \frac{1-\alpha}{1+\alpha}T_1. \tag{6}$$

The magnitudes of the interfacial stress intensity factor K and the T-stresses are linear in the remote load, and also depend upon the detailed geometry of the interfacial crack problem in hand.

A pre-existing interfacial edge crack may propagate along the interface or it may kink into material 1 above the interface or into material 2 below the interface. Continued growth

along the interface is preferred when the toughness of the interface is much lower than that of the two solids. Note that the T-stresses (T_1 in material 1 and T_2 in material 2) have no influence upon G_I for continued interfacial crack growth. When the interface is tougher than either solid, or when the interfacial stress intensity factor has a significant mode II component, the interfacial crack may kink into either of the adjacent materials. He and Hutchinson (1989) and He *et al.* (1991) have developed a precise criterion for the onset of kinking. In their analysis they assume, without loss of generality, that a kink-like flaw of length s exists in material 2 at an angle ω to the interface, as shown in Fig. 3. The putative length s of the kinked crack is taken to be very small compared with all other geometric length scales including the length ℓ of the parent interfacial crack.

Now define a phase angle of loading at the tip of the parent interfacial crack $\bar{\psi}$ by

$$\bar{\psi} = \arctan\left[\frac{\mathrm{Im}\,(Ks^{i\varepsilon})}{\mathrm{Re}\,(Ks^{i\varepsilon})}\right] = \hat{\psi} + \varepsilon \ln\left(\frac{s}{\hat{\ell}}\right). \tag{7}$$

The phase angle $\bar{\psi}$ is based on the length scale s, and gives the ratio of shear stress σ_{xy} to normal stress σ_{yy} at a distance s directly ahead of the interfacial crack tip, $\bar{\psi} = \arctan(\sigma_{xy}/\sigma_{yy})_{r=s}$. Kinking of the interfacial crack into material 2 (the substrate) is governed by the criterion (He and Hutchinson, 1989)

$$\frac{\Gamma_I(\bar{\psi})}{\Gamma_S} > \frac{G_I}{G_S^{max}} \tag{8}$$

where $\Gamma_I(\bar{\psi})$ is the toughness of the interface at a phase angle $\bar{\psi}$ defined in (7), and Γ_S is the mode I toughness of material 2 containing the kink. G_I is the strain energy release rate for continued growth of the interfacial crack, and G_S^{max} is the maximum strain energy release rate for the kinked crack over the full range of $\omega > 0$. The energy criterion (8) is based on the hypothesis that kinking occurs along a direction ω such that the strain energy release rate at the tip of the kink is maximised. The ratio G_I/G_S^{max} depends upon the elastic mismatch parameters (α, β), the phase angle $\bar{\psi}$ and upon the level of in-plane T-stress T_2 parallel to the interface at the crack tip, parameterised by (He *et al.*, 1991)

$$\eta \equiv \frac{T_2\sqrt{s}}{\sqrt{E^* G_I}}. \tag{9}$$

For given values of (α, β) and $\bar{\psi}$, G_I/G_S^{max} decreases with increasing η, as shown in Fig. 4. Note that $|\eta|$ increases with increasing length s of the kinked crack. Therefore, a positive value of η both encourages kinking of an interfacial crack and causes the kinked crack to grow unstably under fixed remote loading. Further, for $\eta > 0$, the subsequent crack trajectory of the kink is expected to diverge from the interface; kink growth is directionally unstable for $\eta > 0$ (Cotterell and Rice, 1980). A negative value of η stabilises an interfacial crack against kinking and may cause a kinked crack to arrest. Also, for $\eta < 0$, crack growth from the initial kink is expected to converge towards the interface and be directionally stable.

Typically, the interfacial toughness $\Gamma_I(\bar{\psi})$ is observed to increase with increasing magnitude of the phase angle $\bar{\psi}$ [see, for example, Cao and Evans (1989); Akisanya and Fleck (1992)]. A representative material response $\Gamma_I(\bar{\psi})/\Gamma_S$ is included in Fig. 4 for the purposes of discussion of the practical utility of the criterion (8). Consider the curve G_I/G_S^{max} for $\eta = 0$ in Fig. 4. The $\Gamma_I(\bar{\psi})/\Gamma_S$ curve crosses the G_I/G_S^{max} curve at $\bar{\psi} \approx 40°$. Thus, kinking is predicted for $\bar{\psi} \geqslant 40°$, but not for $\bar{\psi} < 40°$. Next, consider the G_I/G_S^{max} curve for the case $\eta = 0.2$. This curve crosses the $\Gamma_I(\bar{\psi})/\Gamma_S$ response at $\hat{\psi} \approx 30°$; we expect kinking for $\bar{\psi} \geqslant 30°$ but not for $\bar{\psi} < 30°$. So far we have discussed kinking into material 2. The case of kinking into material 1 (the film) follows immediately upon replacing Γ_S by the mode I toughness

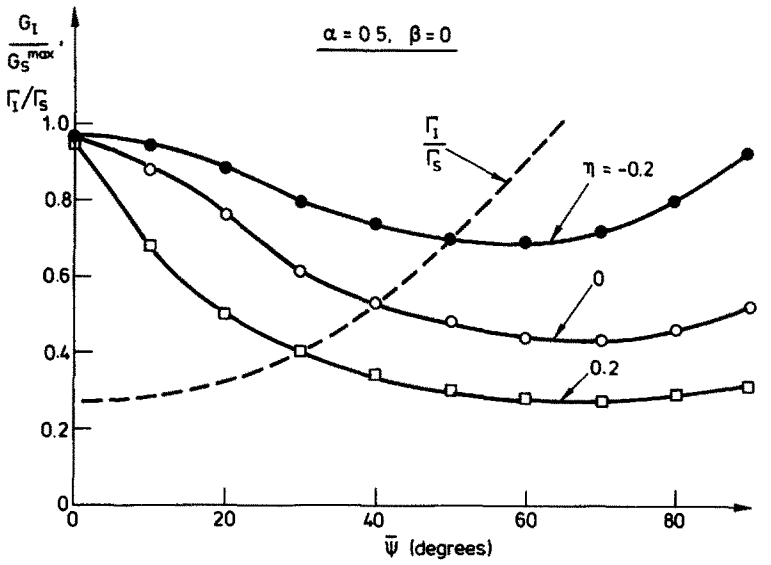

Fig. 4. Effect of the interfacial phase angle $\bar{\psi} = \arctan[\mathrm{Im}(Ks^{ie})/\mathrm{Re}(Ks^{ie})]$ and the normalised T-stress $\eta = T_2\sqrt{s}/\sqrt{E^* G_I}$ upon the ratio G_I/G_S^{max}. G_I is the energy release rate for the interfacial crack, G_S^{max} is the maximum energy release rate for the kinked crack, and s is the length of the kink. Γ_I/Γ_S is a representative normalised interfacial toughness response, where Γ_S is the mode I toughness of the substrate.

of the film Γ_f and by changing the signs of α, β and $\bar{\psi}$. Also, in the evaluation of the normalised T-stress η in eqn (9), T_2 is replaced by T_1 for kinking into material 1.

Later in this paper we shall give the interfacial crack solution for the edge crack geometry and edge loading shown in Fig. 2(c). The crack solution is used to calculate values of η and $\bar{\psi}$, and the likelihood of kinking is then evaluated. In presenting interfacial stress intensity solutions for the edge crack it is convenient to define a phase angle ψ in relation to the film thickness h by

$$\tan\psi = \frac{\mathrm{Im}(Kh^{ie})}{\mathrm{Re}(Kh^{ie})}. \tag{10}$$

Note that ψ is related to $\bar{\psi}$ by

$$\psi = \bar{\psi} + \varepsilon \ln\left(\frac{h}{s}\right) \tag{11a}$$

and is related to $\bar{\psi}$ by

$$\psi = \hat{\psi} + \varepsilon \ln\left(\frac{h}{\hat{\ell}}\right). \tag{11b}$$

2.1. *Condition for the existence of a mode I kink path*

The energy criterion (8) is based on the hypothesis that kinking occurs along a direction ω where the energy release rate at the tip of the kink is maximised. For most values of (α, β) and of phase angle $\bar{\psi}$, this path is almost identical to a mode I kink path (i.e. $K_{II} = 0$ at the kink tip). For an interfacial flaw to grow away from the interface and into substrate (as shown in Fig. 3), the stress intensity factors at the tip of the flaw must satisfy the additional *necessary* condition $K_I > 0$, $K_{II} \geq 0$. A flaw with $K_I < 0$ remains closed and does not grow; a flaw with $K_{II} < 0$ is driven back towards the interface. He *et al.* (1991) have evaluated the stress intensity factors K_I and K_{II} at the tip of a kinked flaw as a function of the flaw

orientation ω, the elastic mismatch parameters (α, β), the phase angle $\bar{\psi}$, and the normalised T-stress η. Using their results we examine the effects of $\bar{\psi}$ and η upon the existence of a mode I kink path in the film and in the substrate.

Define $\bar{\psi}_{c2}$ as the critical phase angle for which the stress intensity factor at the tip of a flaw in material 2 (the substrate) with a vanishingly small orientation $\omega = 0^+$ satisfies the condition $K_I > 0$, $K_{II} = 0$. When $|\eta| \leqslant 0.8$ and $\bar{\psi} = \bar{\psi}_{c2}$, a single mode I kink path exists in the substrate oriented tangentially to the interface. For $|\eta| > 0.8$ and $\bar{\psi} = \bar{\psi}_{c2}$, an additional kink path exists at finite ω such that $K_{II} = 0$ and K_I is larger than that along the $\omega = 0$ path. In the present study we restrict discussion to the simpler case $|\eta| \leqslant 0.8$. (We shall show later that for realistic residual stress distributions in the film, the magnitude of the normalised T-stress η is less than 0.8 for most film/substrate systems.) The critical phase angle $\bar{\psi}_{c2}$ depends only upon the material elastic parameters α and β since a crack at $\omega = 0^+$ or 0^- is not influenced by the T-stress; typical results are given in Fig. 5 for the case $\beta = 0$. The figure also shows the critical phase angle for which a mode I kink path exists in material 1 and lies parallel to the interface.

When $\bar{\psi} > \bar{\psi}_{c2}$, a mode I kink path exists at a finite angle ω in material 2 (the substrate) and kinking into the substrate is predicted if the energy condition (8) is satisfied. For such values of $\bar{\psi}$ $(> \bar{\psi}_{c2})$ now consider the possibility of kinking into material 1 (the film) above the interface; K_{II} is positive for all flaws in material 1 for which $K_I > 0$ and a kink in material 1 propagates back to the interface.

In a similar manner define $\bar{\psi}_{c1}$ as the critical phase angle for which the stress intensity factors at the tip of a flaw in material 1 (the film) and oriented tangentially to the interface satisfies the condition $K_I > 0$, $K_{II} = 0$. Then, a mode I kink path exists in material 1 provided $\bar{\psi} < \bar{\psi}_{c1}$, and kinking into material 1 is predicted if the energy condition is satisfied. For a small range in $\bar{\psi}$ of less than 3°, a mode I path exists in both materials 1 and 2. We ignore this subtlety and assume in our application of the He and Hutchinson analysis that a mode I path exists in the substrate for $\bar{\psi} > \bar{\psi}_{c2}$ and in the film for $\bar{\psi} < \bar{\psi}_{c2}$. For a given value of (α, β) and $|\eta| \leqslant 0.8$, the critical phase angle $\bar{\psi}_c \equiv \bar{\psi}_{c2}$ marks the transition from the existence of a mode I path in the substrate to the existence of a mode I path in the film. The effect of phase angle $\bar{\psi}$ (for $|\eta| \leqslant 0.8$) upon crack path selection is summarised schematically in Fig. 6, assuming that sufficient energy exists to grow in the kink.

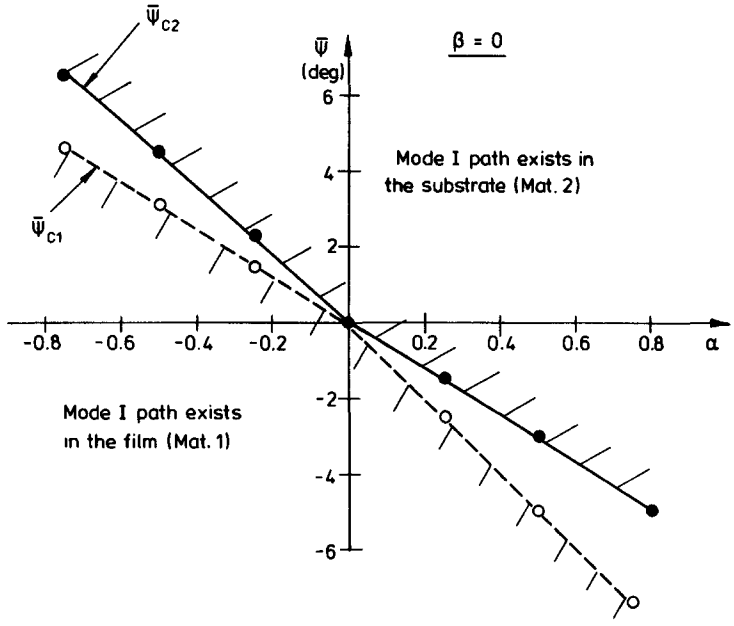

Fig. 5. Effect of elastic mismatch parameters (α, β) upon the critical phase angle $\bar{\psi}_c$ at which a mode I kink path ($K_I > 0$, $K_{II} = 0$) exists tangentially to the interface.

3. STRESS INTENSITIES AND T-STRESSES FOR INTERFACIAL EDGE CRACK

The finite element method is used to analyse the plane elasticity problem shown in Fig. 2(c). An elastic film of thickness h is deposited on an elastic substrate of thickness H. Both the film and the substrate are isotropic elastic solids, but the elastic constants of the film (material 1) in general differ from those of the substrate (material 2). An interfacial crack of length ℓ exists at each edge of the film/substrate system. The origin of the rectangular co-ordinate system (x, y) is at the left hand crack tip such that the interface is along $y = 0$ and the free surface of the film is along $y = h$.

The magnitude of the stress increases linearly from a value of $\sigma = \sigma_1$ at the interface ($y = 0$) to a value of $\sigma = \sigma_2$ at the free surface of the film ($y = h$). Thus, the variation of compressive normal stress σ at the edge of the film is given by

$$\sigma(y) = \sigma_1 + (\sigma_2 - \sigma_1)(y/h). \tag{12}$$

The loading shown in Fig. 2(c) is equivalent to a force per unit thickness P and a moment per unit thickness M, acting at the mid-plane of the film ($y = h/2$) as shown in bold face in Fig. 2(c). The loads P and M are given by

$$P = \bar{\sigma} h \tag{13a}$$

$$M = \tfrac{1}{6} h^2 \Delta\sigma, \tag{13b}$$

where

$$\bar{\sigma} = \tfrac{1}{2}(\sigma_1 + \sigma_2) \qquad \text{and} \qquad \Delta\sigma = \tfrac{1}{2}(\sigma_2 - \sigma_1). \tag{14}$$

For the case of a uniform stress in the film, $\sigma_1 = \sigma_2 = \sigma_0$ is equivalent to $P = \bar{\sigma} h = \sigma_0 h$ and $M = 0$.

For an arbitrary combination of P and M, the stress field at the tip of the interfacial crack of length ℓ from the edge is governed by the complex interfacial stress intensity factor K and the T-stresses T_1 in material 1 (the film) and T_2 in material 2 (the substrate). Dimensional considerations require that the stress intensity factor and the T-stresses are related to the geometry and the load quantities P and M by

$$Kh^{i\varepsilon} = aPh^{-1/2} + bMh^{-3/2} \tag{15}$$

$$T_1 = cPh^{-1} + dMh^{-2}. \tag{16}$$

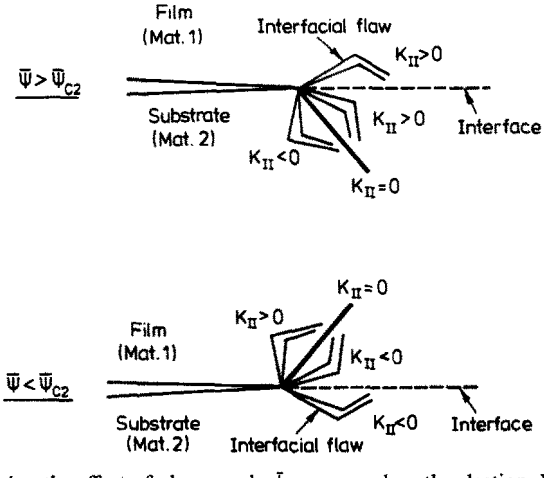

Fig. 6. Sketch showing the effect of phase angle $\bar{\psi}$ upon crack path selection. We assume that the mode I stress intensity factor at the flaw tip K_I is positive, and that sufficient energy exists to drive the kink.

Here a, b, c and d are non-dimensional functions of the elastic mismatch parameters (α, β) relative crack length ℓ/h, and of the ratio of film to substrate thickness h/H. The parameters a and b are complex, while c and d are real. The T-stress T_2 in material 2 (substrate) is related to the T-stress T_1 in material 1 (film) via eqn (6).

The elastic strain energy release rate G_I for interfacial crack growth is given by

$$E^*G_I = |K|^2 = |Kh^{ie}|^2, \tag{17}$$

where the subscript I denotes the interface and E^* is a function of the elastic properties defined in Section 2. By substituting for Kh^{ie} from eqn (15) into eqn (17), G_I can be expressed in the dimensionless form

$$\frac{hE^*G_I}{P^2} = a\bar{a} + \left(\frac{M}{Ph}\right)(\bar{a}b + a\bar{b}) + b\bar{b}\left(\frac{M}{Ph}\right)^2, \tag{18}$$

where the overbar denotes the complex conjugate.

4. NUMERICAL ANALYSIS

We examine by the finite element method the effect of the geometrical parameters ℓ/h and h/H, material parameters (α, β), and the non-dimensional loading parameter M/Ph upon the interfacial stress intensity factor, energy release rate and the T-stresses. Unless otherwise stated, the discussion is restricted to the case $h/H = 0.01$. Numerical computations were performed for a thin film/substrate system having a length $L = 100h$, where h is the thickness of the film, as shown in Fig. 2(c). Three values of the substrate thickness H are considered: $H = 3h$, $10h$ and $100h$. The end face of the film is loaded such that the stress variation across the thickness of the film is given by eqn (12).

Both the stress intensity factor and the interfacial T-stress are determined by:

(i) evaluating the path-independent J integral for the elastic state of interest, followed by
(ii) evaluating the J integral for the linear superposition of the elastic state of interest and a suitably chosen auxiliary elastic field (Kfouri, 1986; Matos *et al.*, 1989).

Parks' (1974) virtual crack extension method is used to evaluate the path-independent J integral. For evaluation of the components K_1 and K_2 of the interfacial stress intensity factor, the auxiliary field is taken as the singular crack tip field for an interfacial crack (Matos *et al.*, 1989). In the evaluation of the T-stresses, the auxiliary elastic field consists of a point force placed at the tip of a semi-infinite interfacial crack and in a direction parallel to the crack faces (Kfouri, 1986). Further details are given in the Appendix.

An elastic analysis has been carried out using the finite element code MARC-K3 (MARC-CDC, 1974). The finite element mesh consists of between 600 and 1100 eight-noded plane strain isoparametric, quadrilateral elements depending upon the relative crack length ℓ/h and the ratio of film to substrate thickness h/H. A typical finite element mesh is shown in Fig. 7. Roller boundary conditions are imposed along the mid-plane of the double edge cracked configuration, as dictated by symmetry requirements.

The coefficients a, b, c and d in eqns (15) and (16) are determined by applying the two loads P and M in turn. Results are listed in Table 1 for the material parameters $\alpha = -0.5$, 0, 0.5 and $\beta = \alpha/4$, relative crack lengths $0.1 \leqslant \ell/h \leqslant 20$, and relative film to substrate thicknesses $0.01 \leqslant h/H \leqslant 0.3$. Results for other values of α and β ($= 0$ and $\alpha/4$) are reported elsewhere in Akisanya and Fleck (1993). A comparison of the results at large relative crack lengths $\ell/h = 20$ with existing steady state solutions (Suo and Hutchinson, 1990) shows that the results are accurate to within about 1%.

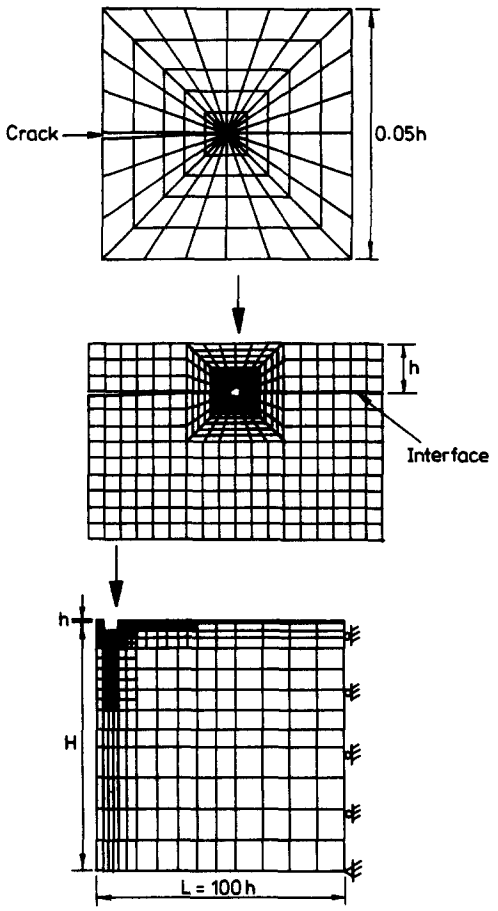

Fig. 7. The finite element mesh.

5. RESULTS

5.1. *Strain energy release rate and phase angle*

The strain energy release rate G_I for the interfacial crack is given by eqn (18), and the phase angle ψ is given via eqns (10) and (15) as

$$\psi = \arctan\left(\frac{\mathrm{Im}\,(Kh^{ie})}{\mathrm{Re}\,(Kh^{ie})}\right) = \arctan\left(\frac{\mathrm{Im}\,(aPh^{-1/2}+bMh^{-3/2})}{\mathrm{Re}\,(aPh^{-1/2}+bMh^{-3/2})}\right). \tag{19}$$

Once the calibration functions a and b have been deduced from the finite element analysis (for any given values of ℓ/h, h/H, α and β), the quantities G_I and ψ are known for any prescribed loading P and M by making use of eqns (18) and (19).

Results for G_I and ψ are given in Fig. 8 for the cases of a pure end load P and for a pure moment M. Values for G_I have been normalised by the steady state value G_I^∞ for a single, semi-infinite interfacial crack between a thin film and an infinitely thick substrate ($h/H \approx 0$), as found by Suo and Hutchinson (1990). For pure end loading P, G_I^∞ is given by $G_I^\infty = P^2/2\bar{E}_1 h$, while for a pure moment M the steady state energy release rate is $G_I^\infty = 6M^2/\bar{E}_1 h^3$. Interfacial toughness data are commonly presented in the G_I–ψ plane. Thus it is instructive to present our results by taking G_I/G_I^∞ and ψ as axes in Fig. 8. Each curve is for a prescribed (α, β) value, and is a trajectory for ℓ/h in the range of 0.1 to 20. To within the numerical accuracy of the calculations (about 1% error), a steady state has been achieved for ψ by the stage $\ell/h = 3$, and a steady state has been achieved for G_I by the stage $\ell/h = 20$.

Table 1. Tabulated solution for the coefficients $a = a_R + i\,a_I$, $b = b_R + i\,b_I$, c and d: (a) $\alpha = -0.5$, $\beta = \alpha/4$; (b) $\alpha = 0$, $\beta = 0$; (c) $\alpha = 0.5$; $\beta = \alpha/4$

(a)

		c			d			a_R			a_I			b_R			b_I	
ℓ/h	0.01	0.10	0.33	0.01	0.10	0.33	0.01	0.10	0.33	0.01	0.10	0.33	0.01	0.10	0.33	0.01	0.10	0.33
0.1	−0.363	−0.378	−0.394	1.076	0.997	0.960	0.320	0.323	0.307	0.359	0.355	0.263	1.956	1.960	1.290	−1.154	−1.165	−1.238
0.3	−0.303	−0.321	−0.335	1.253	1.202	1.185	0.354	0.357	0.313	0.498	0.491	0.380	2.427	2.429	2.019	−1.625	−1.631	−1.338
0.5	−0.258	−0.278	−0.306	1.266	1.173	1.164	0.383	0.387	0.324	0.552	0.550	0.419	2.444	2.454	2.086	−1.717	−1.734	−1.895
0.8	−0.215	−0.238	−0.267	1.219	1.130	1.115	0.413	0.417	0.423	0.589	0.587	0.442	2.436	2.451	2.154	−1.742	−1.756	−2.004
1.0	−0.195	−0.213	−0.239	1.203	1.118	1.111	0.427	0.433	0.374	0.604	0.607	0.476	2.431	2.451	2.223	−1.749	−1.767	−2.114
3.0	−0.122	−0.150	−0.229	1.164	1.076	1.083	0.471	0.470	0.377	0.656	0.652	0.478	2.421	2.448	2.265	−1.768	−1.787	−1.856
6.0	−0.096	−0.140	−0.229	1.158	1.070	1.084	0.486	0.474	0.378	0.675	0.659	0.479	2.419	2.450	2.284	−1.772	−1.791	−1.974
10.0	−0.083	−0.140	−0.227	1.157	1.074	1.076	0.493	0.475	0.379	0.684	0.658	0.484	2.418	2.447	2.303	−1.773	−1.786	−1.982
15.0	−0.077	−0.139	−0.227	1.156	1.069	1.084	0.496	0.474	0.380	0.689	0.689	0.480	2.418	2.447	2.374	−1.773	−1.789	−1.985
20.0	−0.073	−0.139	−0.226	1.156	1.069	1.077	0.498	0.474	0.380	0.691	0.659	0.483	2.418	2.446	2.374	−1.773	−1.790	−2.017

(b)

		c			d			a_R			a_I			b_R			b_I	
ℓ/h	0.01	0.10	0.33	0.01	0.10	0.33	0.01	0.10	0.33	0.01	0.10	0.33	0.01	0.10	0.33	0.01	0.10	0.33
0.1	−0.582	−0.585	−0.569	2.179	2.028	2.041	0.108	0.110	0.096	0.183	0.176	0.131	1.694	1.708	1.690	−1.022	−1.007	−1.168
0.3	−0.548	−0.550	−0.534	2.556	2.478	2.417	0.182	0.182	0.142	0.287	0.274	0.230	1.929	1.936	1.908	−1.355	−1.352	−1.768
0.5	−0.498	−0.510	−0.502	2.598	2.429	2.461	0.226	0.227	0.180	0.334	0.327	0.256	1.924	1.914	1.915	−1.418	−1.439	−1.439
0.8	−0.441	−0.457	−0.503	2.530	2.360	2.332	0.268	0.267	0.190	0.374	0.366	0.318	1.913	1.913	1.857	−1.444	−1.458	−1.443
1.0	−0.412	−0.431	−0.454	2.507	2.336	2.328	0.288	0.288	0.198	0.392	0.389	0.305	1.908	1.934	1.692	−1.452	−1.470	−1.489
3.0	−0.292	−0.335	−0.440	2.447	2.271	2.289	0.358	0.343	0.203	0.466	0.448	0.309	1.892	1.902	1.690	−1.478	−1.504	−1.568
6.0	−0.241	−0.318	−0.440	2.436	2.258	2.288	0.386	0.350	0.203	0.499	0.459	0.311	1.888	1.913	1.690	−1.484	−1.505	−1.578
10.0	−0.216	−0.318	−0.440	2.432	2.260	2.285	0.399	0.350	0.203	0.516	0.459	0.312	1.887	1.915	1.688	−1.486	1.503	−1.580
15.0	−0.201	−0.316	−0.439	2.431	2.248	2.278	0.407	0.350	0.204	0.525	0.460	0.316	1.886	1.919	1.729	−1.487	−1.508	−1.608
20.0	−0.193	−0.318	−0.438	2.431	2.261	2.277	0.411	0.350	0.205	0.530	0.460	0.318	1.886	1.909	1.720	−1.487	−1.514	−1.610

(c)

		c			d			a_R			a_I			b_R			b_I	
ℓ/h	0.01	0.10	0.33	0.01	0.10	0.33	0.01	0.10	0.33	0.01	0.10	0.33	0.01	0.10	0.33	0.01	0.10	0.33
0.1	−0.748	−0.714	−0.591	3.528	3.323	3.529	−0.006	−0.005	−0.018	0.096	0.088	0.063	1.283	1.265	1.382	−0.826	−0.850	−1.010
0.3	−0.758	−0.796	−0.595	3.998	3.934	3.997	0.051	0.051	0.025	0.143	0.131	0.093	1.390	1.386	1.457	−0.973	−0.946	−1.068
0.5	−0.728	−0.700	−0.579	4.063	3.841	3.966	0.086	0.086	0.044	0.170	0.162	0.121	1.390	1.372	1.483	−0.997	−1.013	−1.073
0.8	−0.683	−0.660	−0.660	4.005	3.786	3.815	0.120	0.117	0.058	0.197	0.186	0.152	1.387	1.394	1.422	−1.012	−1.020	−1.096
1.0	−0.658	−0.663	−0.640	3.987	3.749	3.789	0.137	0.135	0.069	0.211	0.204	0.151	1.383	1.405	1.381	−1.017	−1.038	−1.126
3.0	−0.537	−0.576	−0.630	3.934	3.679	3.729	0.207	0.182	0.070	0.281	0.253	0.154	1.373	1.387	1.349	−1.038	−1.066	−1.164
6.0	−0.472	−0.560	−0.630	3.921	3.661	3.716	0.240	0.188	0.071	0.319	0.262	0.157	1.369	1.394	1.355	−1.044	−1.071	−1.197
10.0	−0.434	−0.563	−0.635	3.917	3.674	3.724	0.258	0.189	0.073	0.342	0.262	0.157	1.367	1.379	1.317	−1.047	−1.067	−1.244
15.0	−0.410	−0.560	−0.637	3.913	3.652	3.670	0.269	0.188	0.073	0.356	0.263	0.158	1.366	1.388	1.349	−1.048	−1.069	−1.250
20.0	−0.397	−0.562	−0.639	3.913	3.661	3.722	0.275	0.188	0.073	0.364	0.263	0.159	1.366	1.387	1.347	−1.049	−1.068	−1.258

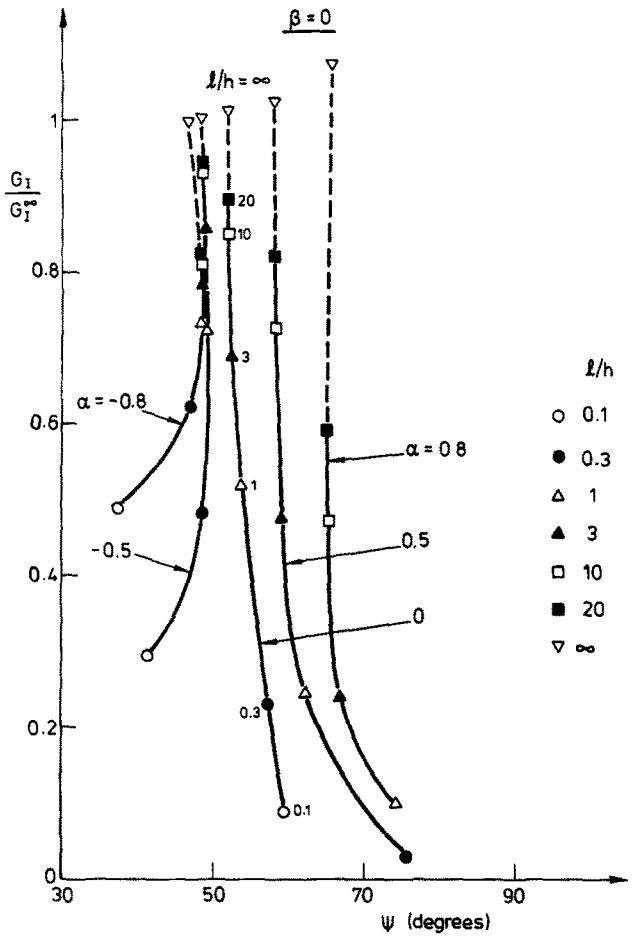

Fig. 8. The effect of the elastic mismatch parameters (α, β) and relative crack length ℓ/h upon the normalised energy release rate G_1/G_1^{∞} and the phase angle

$$\psi = \arctan\left[\frac{\mathrm{Im}(Kh^{i\varepsilon})}{\mathrm{Re}(Kh^{i\varepsilon})}\right].$$

Loading is a pure end load P for (a) $\beta = 0$ and (b) $\beta = \alpha/4$ and a pure end moment M for (c) $\beta = 0$ and (d) $\beta = \alpha/4$. Note that $G_1^{\infty} = P^2/(2\bar{E}_1 h)$ in (a) and (b), and $G_1^{\infty} = 6M^2/(\bar{E}_1 h^3)$ in (c) and (d), where $\bar{E}_1 = E_1/(1-\upsilon_1^2)$ is the plane strain modulus of the film. The asymptotic values for G_1/G_1^{∞} and ψ at $\ell/h = \infty$ are given by Suo and Hutchinson (1990).

It is clear from Figs 8(a–d) that the dominant effect of increasing ℓ/h from zero is to increase G_1/G_1^{∞} from zero to the steady state value, with little attendant change in ψ. This suggests that interfacial crack growth is unstable under fixed remote loading. For all values of (α, β), the phase angle ψ asymptotes to a steady state value in the range 40° to 60° for pure end loading P, and to a value in the range −45° to −25° for a pure end moment M. Clearly, under combined loading P and M, a wide range of values is achievable for ψ. The effect of the material mismatch parameter β upon the values of G_1/G_1^{∞} and ψ is minor.

5.2. *Interfacial stress intensity factor*

The components of the interfacial stress intensity factor defined by eqn (15) can be expressed in non-dimensional form as

$$\frac{\mathrm{Re}(Kh^{i\varepsilon})}{Ph^{-1/2}} = a_R + b_R \frac{M}{Ph} \tag{20a}$$

$$\frac{\mathrm{Im}(Kh^{i\varepsilon})}{Ph^{-1/2}} = a_I + b_I \frac{M}{Ph}, \tag{20b}$$

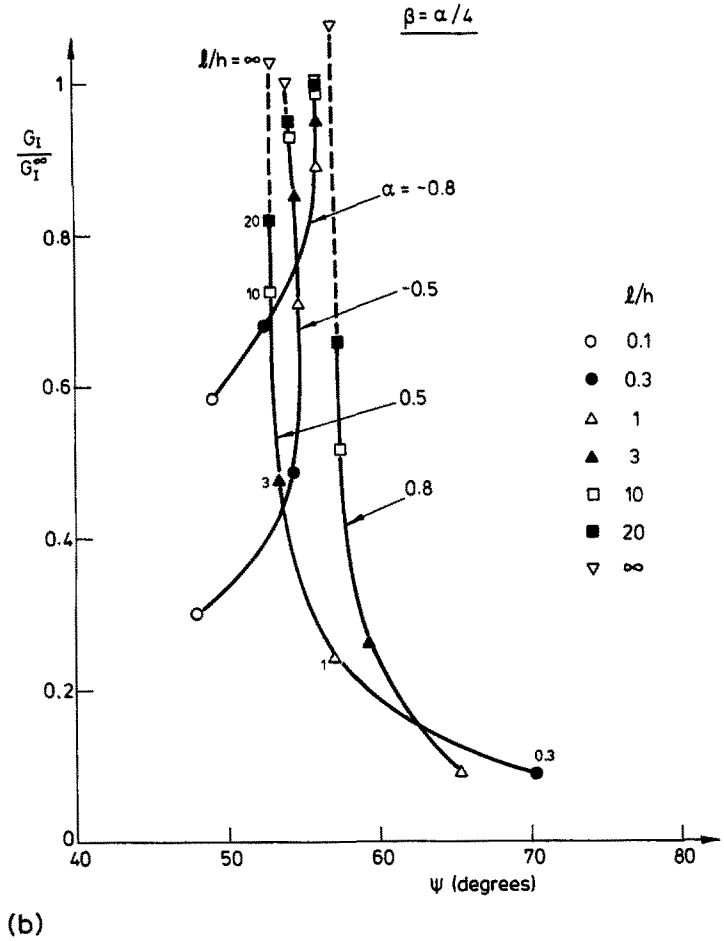

Fig. 8(b). *Continued.*

where a_R and a_I are the real and imaginary parts of the complex coefficient a; similarly, b_R and b_I are the real and imaginary parts of the complex coefficient b.

Figure 9 displays the critical value of the non-dimensional loading ratio M/Ph at which the opening component of the stress intensity factor [i.e. $\mathrm{Re}(Kh^{ie})$] vanishes, for a given crack length ℓ/h. When M/Ph exceeds the critical value, crack growth is possible; when M/Ph is less than the critical value, the crack tip is closed and no crack growth is expected. Figure 9 also shows that for sufficiently negative values of M/Ph and for sufficiently negative values of α, a crack of length $\ell/h < 1$ is stable under fixed remote load; the opening component of the stress intensity factor decreases to zero as the crack advances. For sufficiently positive values of M/Ph, the crack tip remains open for all values of crack length.

As an example consider a film under a uniform compressive edge load such that $M/Ph = 0$. For the case $\alpha = \beta = 0$ (i.e. homogeneous solid), the crack tip is open for all values of ℓ/h. For $\alpha = 0.8$ and $\beta = \alpha/4$, the crack tip is closed for $\ell/h < 0.3$, and crack growth is inhibited. Thus, Fig. 9 serves as a design guide for the domain of safe residual stress distribution in the film such that crack growth is not possible, for any assumed value of interfacial crack length.

5.3. *The interfacial* T-*stress*

Figure 10 shows the normalised T-stresses T_1h/P and T_1h^2/M in material 1 (i.e. the film) due to the loading P and M, respectively, as a function of the relative crack length ℓ/h. The corresponding normalised T-stresses T_2h/P and T_2h^2/M in material 2 (the substrate) are obtained via eqn (6). Although T_1 and T_2 have the same sign, the absolute value of T_2 is higher than the absolute value of T_1 when $\alpha < 0$, and is lower than the absolute value of T_1 when $\alpha > 0$. We observe that T_1h/P due to load P is negative while T_1h^2/M due to M is

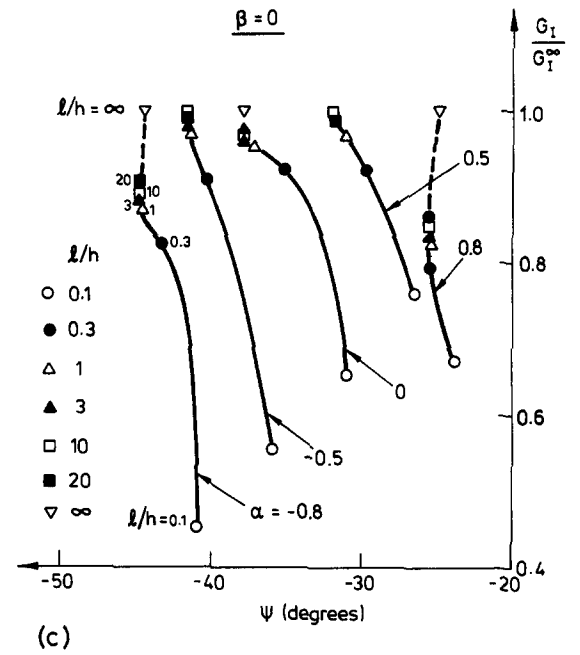

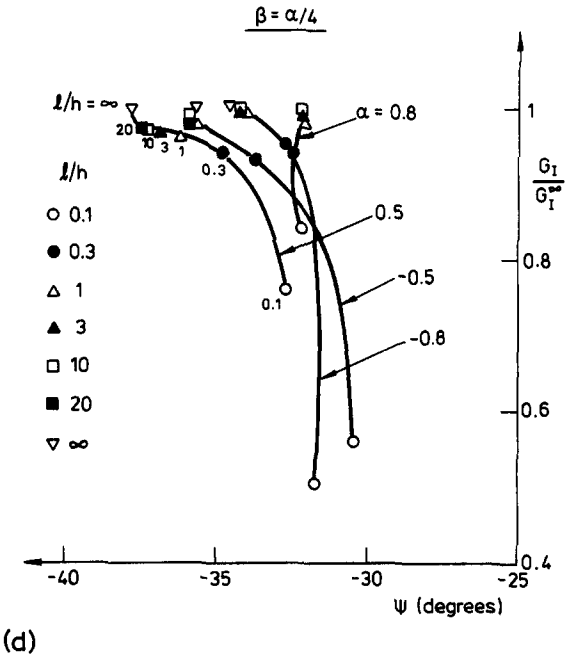

Figs 8(c) and (d). *Continued.*

positive for all values of the material parameters (α, β) and relative crack length ℓ/h considered. There is an appreciable increase in $T_1 h/P$ in the interval $0 < \ell/h < 6$ until a steady state is attained at $\ell/h > 6$; $T_1 h^2/M$ shows a small local maximum at $\ell/h \approx 0.5$, and attains a steady state at $\ell/h > 1$. The effect of the β-value on the T-stress due to either P or M is negligible.

The normalised T-stress $\eta \equiv (T_2\sqrt{s})/\sqrt{E^* G_I}$ for kinking into the substrate (material 2) has been evaluated for an assumed relative flaw size s/h and for a range of values of M/Ph. Recall that a positive value of the normalised T-stress η encourages the kinking of an interfacial crack. The variation of η with crack length is shown in Fig. 11(a) for the case $\alpha = \beta = 0$ and $s/h = 0.01$; η increases with the normalised interfacial crack length ℓ/h until

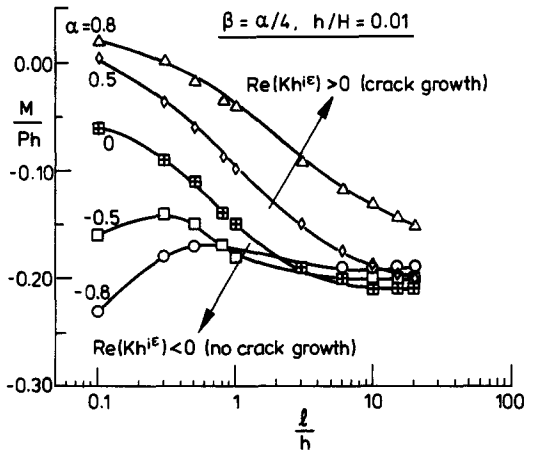

Fig. 9. The non-dimensional loading parameter M/Ph at which $\mathrm{Re}(Kh^{i\varepsilon}) = 0$, plotted as a function of relative crack length ℓ/h and the elastic mismatch parameters α and β ($= \alpha/4$).

steady state is attained, and also increases with increasing M/Ph. The critical value of M/Ph at which $\eta = 0$ is shown in Fig. 11(b) as a function of the non-dimensional crack length ℓ/h, for α in the range -0.8 to 0.8 (with $\beta = \alpha/4$). It is clear from Fig. 11(b) that for sufficiently large and positive values of M/Ph, η is positive for all values of ℓ/h. The effect

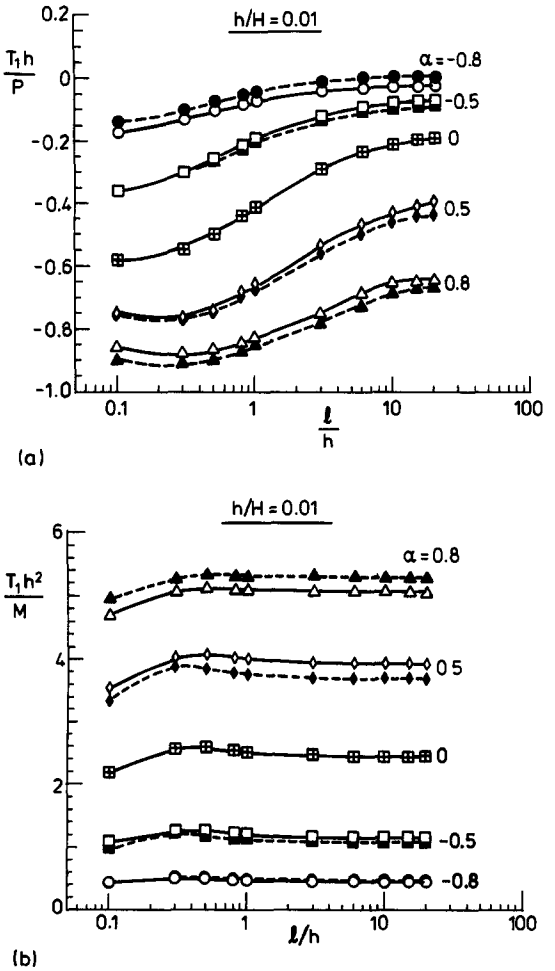

Fig. 10. The effect of relative crack length ℓ/h and elastic mismatch parameters (α, β) upon the normalised T-stress in the film, due to (a) a pure end load P and (b) a pure end moment M. The filled symbols refer to $\beta = 0$, and the open symbols refer to $\beta = \alpha/4$.

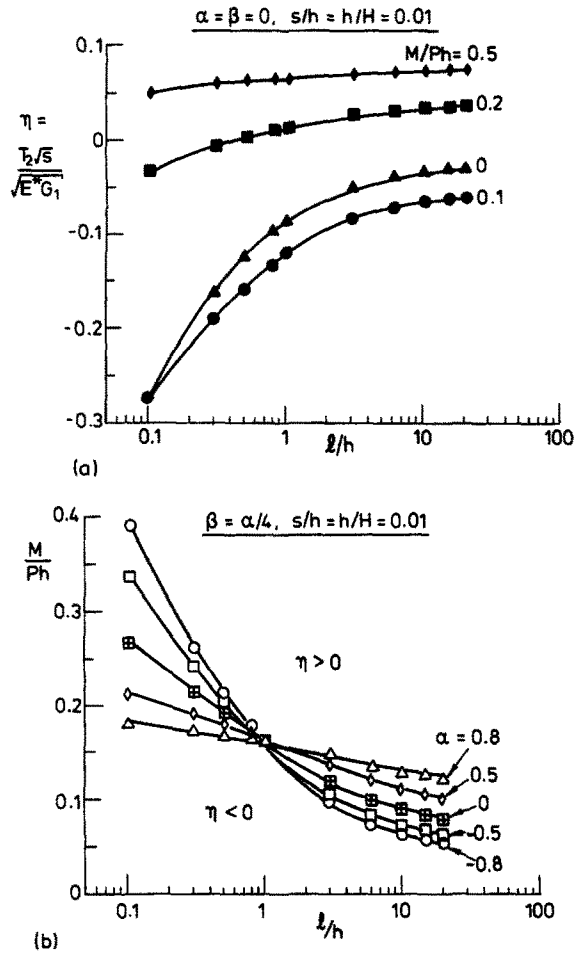

Fig. 11. (a) The normalised T-stress $\eta = T_2\sqrt{s}/\sqrt{E^*G_1}$ as a function of relative crack length ℓ/h and loading parameter M/Ph, for $\alpha = \beta = 0$, $s/h = 0.01$ and $h/H = 0.01$. (b) The non-dimensional loading parameter M/Ph at which the T-stress $T_1 = T_2 = 0$, plotted as a function of relative crack length ℓ/h and elastic mismatch parameters α and $\beta(= \alpha/4)$.

of the elastic mismatch parameters (α, β) on the critical value of M/Ph at which η changes sign is only minor for values of $\ell/h \geqslant 1$, as shown in Fig. 11(b).

The absolute value of the loading parameter M/Ph ($= \Delta\sigma/6\bar{\sigma}$) is less than unity for most thin film/substrate systems of technological importance. The corresponding value of $|\eta|$ is less than 0.8 except when ℓ/h is small and M/Ph is large and negative [see, for example, Fig. 11(a)]. Most thin film/substrate systems have M/Ph values in the range $0 \leqslant M/Ph \leqslant 1$. Therefore, the assumption that $|\eta| \leqslant 0.8$ can be made for most thin film/substrate systems.

5.4. *Selection of kink path: into the substrate or film?*

An interfacial edge crack can grow along one of three different paths depending upon the loading condition and the relative value of the ratios Γ_I/Γ_S and Γ_I/Γ_f. Here Γ_I is the mode-dependent toughness of the interface, and Γ_S and Γ_f are the mode I toughnesses of the substrate and film, respectively. The three possible paths are:

(i) continued growth along the interface;
(ii) kinking into the substrate;
(iii) kinking into the film, which may result in spalling of the film.

Kinking into the substrate (or into the film) depends upon the existence of a mode I kink path in the substrate (or in the film) and upon satisfying the energy condition (8), as discussed in Section 2. The *existence* of a mode I kink path depends only upon the phase angle $\hat{\psi}$ when the magnitude of the normalised T-stress η [defined in eqn (9)] is less than

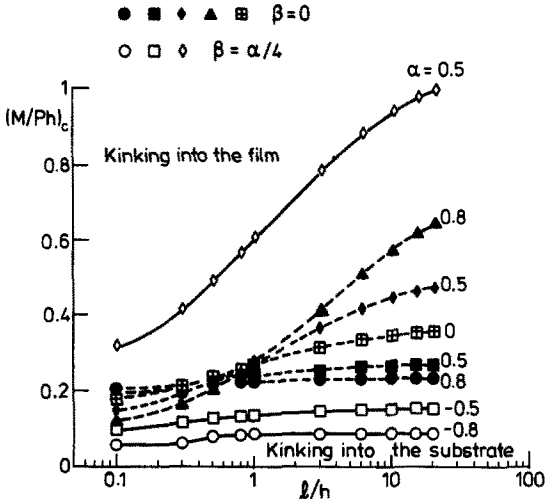

Fig. 12. Effect of the relative crack length ℓ/h upon the critical value of the loading parameter $(M/Ph)_c$ at which kinking switches from the substrate to the film, for a film/substrate thickness ratio $h/H = 0.01$ and a relative flaw size $s/h = 0.01$. $M/Ph = (M/Ph)_c$ when $\psi = \psi_c$. The filled symbols refer to $\beta = 0$, and the open symbols refer to $\beta = \alpha/4$.

0.8. Note that the actual direction of the mode I path is dependent on both $\hat{\psi}$ and η. Recall that a mode I path exists in the substrate when the phase angle $\hat{\psi} \geqslant \hat{\psi}_c$; the critical phase angle $\hat{\psi}_c$ is shown in Fig. 5. The corresponding critical phase angle ψ_c is given by eqn (11a).

We assume that kinking of the interfacial crack into the substrate occurs when $\psi(\alpha, \beta, \ell/h, h/H, M/Ph) \geqslant \psi_c(\alpha, \beta, s/h)$, provided the energy condition (8) is satisfied. We take the equality $\psi(\alpha, \beta, \ell/h, h/H, M/Ph) = \psi_c(\alpha, \beta, s/h)$ in order to deduce the critical value of the ratio of bending to axial compressive load $(M/Ph)_c$ at which kinking switches from the substrate to the film. The results are plotted in Fig. 12, for $h/H = 0.01$, $s/h = 0.01$, and for various values of α (with $\beta = 0$ and $\beta = \alpha/4$). The results plotted in Fig. 12 give a qualitative prediction of crack path for a given thin film/substrate system as discussed below.

For a loading parameter $M/Ph < (M/Ph)_c$ there is, at least, one flaw orientation in the *substrate* for which $K_{II} \geqslant 0$ and $K_I > 0$; the crack kinks into the substrate and grows away from the interface if the values of ψ and η are such that the energy criterion (8) is satisfied. Similarly, when $M/Ph > (M/Ph)_c$, there is, at least, one flaw orientation in the *film* for which $K_{II} \leqslant 0$ and $K_I > 0$.

It is evident from the above discussion that the onset of kinking of a crack at the interface of a given film/substrate system into the substrate or into the film is strongly affected by the values of ψ and the normalised T-stress η. To predict the onset of kinking, the following strategy is adopted. Consider a thin film/substrate system as shown in Fig. 2(c). We assume the mode dependence of the interfacial toughness $\Gamma_I(\psi)$ and the value of the loading parameter M/Ph are known. The present analysis provides the values for phase angle ψ, critical loading parameter $(M/Ph)_c$ and for the normalised T-stress η, based on estimates of initial relative interfacial crack length ℓ/h and flaw size s/h. The calculated values of ψ and η are used to determine G_I/G_S^{max} using the analysis presented by He *et al.* (1991) (see, for example, Fig. 4). Sufficient energy is available for kinking when eqn (8) is satisfied. (For kinking into the film substitute $\Gamma_S = \Gamma_f$ into eqn (8), $T_1 = T_2$ into eqn (9), and the signs of α, β and ψ in eqn (8) are reversed.) Kinking into the substrate is predicted if the non-dimensional loading $M/Ph < (M/Ph)_c$, and kinking into the film occurs if $M/Ph > (M/Ph)_c$, for assumed values of ℓ/h and s/h.

5.5. *Effect of film/substrate thickness ratio upon interfacial cracking response*

The effect of the film/substrate thickness ratio h/H upon the interfacial energy release rate G_I and the phase angle ψ due to pure end load P, is shown in Fig. 13(a); Fig. 13(b) shows the response due to a pure end moment M. The interfacial energy release rate G_I is again normalised by the energy release rate G_I^∞ for a semi-infinite interfacial crack between

a thin film and an infinitely thick substrate ($h/H \approx 0$). The results shown in Figs 13(a) and 13(b) are for a film/substrate combination with material parameters $\alpha = 0.5$ and $\beta = \alpha/4$; the effect of h/H upon the G_I/G_I^∞ versus ψ response for other values of α and β are qualitatively similar to that shown in Figs 13(a) and 13(b).

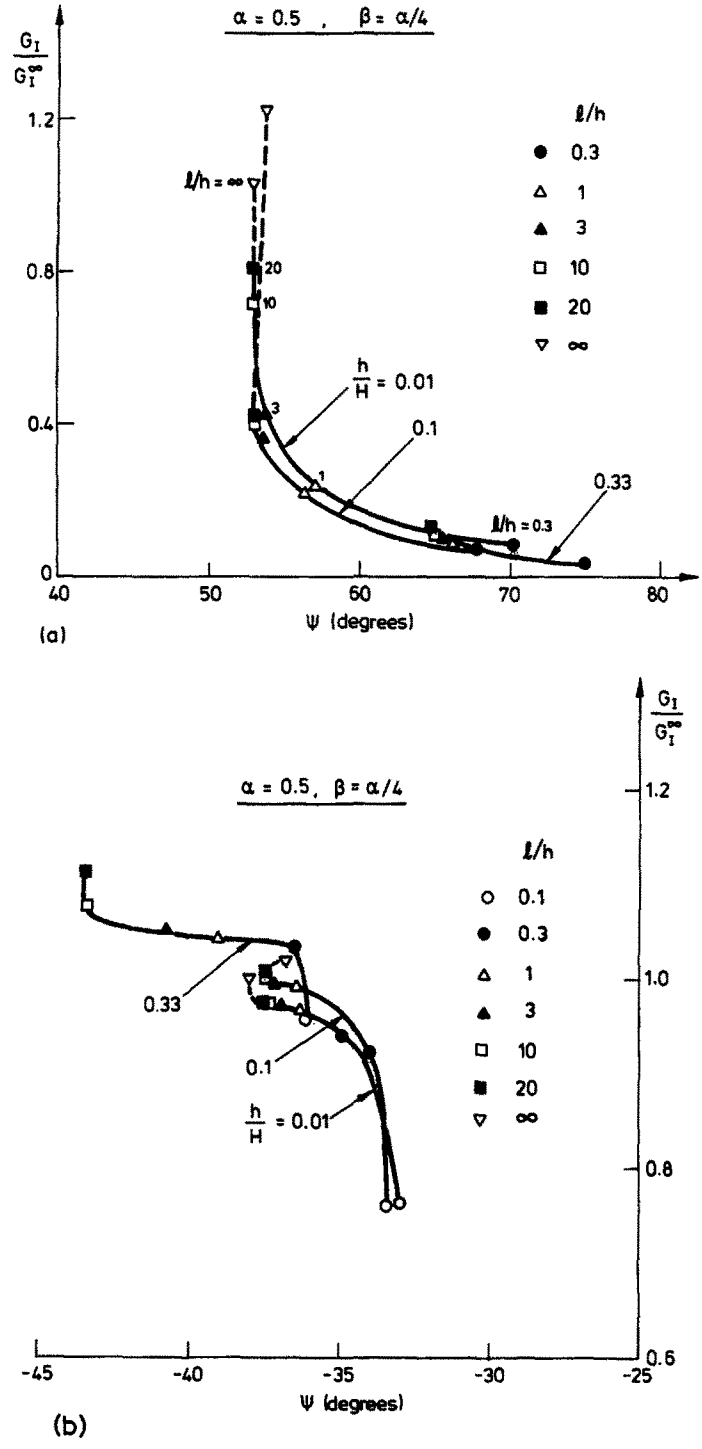

Fig. 13. Effect of thickness ratio h/H upon the normalised energy release rate G_I/G_I^∞ and the phase angle $\psi = \arctan[\mathrm{Im}(Kh^{ie})/\mathrm{Re}(Kh^{ie})]$ due to (a) a pure end load P and (b) a pure end moment M, and upon the normalised T-stress in the film due to (c) a pure end load P and to (d) a pure end moment M. In all cases $\alpha = 0.5$, $\beta = \alpha/4$. Note that $G_I^\infty = P^2/(2\bar{E}_1 h)$ in (a) and $G_I^\infty = 6M^2/(\bar{E}_1 h^3)$ in (b), where $\bar{E}_1 = E_1/(1-\upsilon_1^2)$ is the plane strain modulus of the film. The asymptotic values for G_I/G_I^∞ and ψ at $\ell/h = \infty$ are given by Suo and Hutchinson (1990).

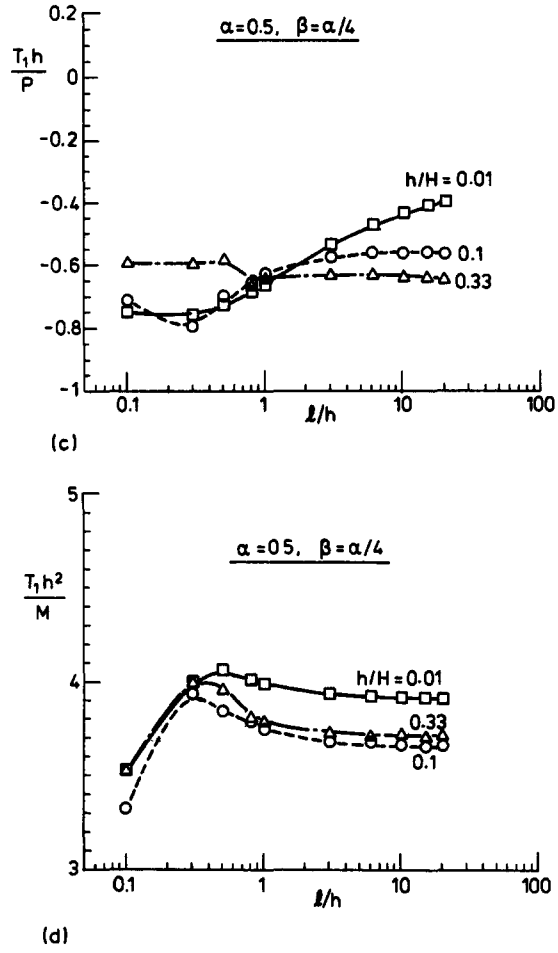

Figs 13(c) and (d). *Continued.*

For a pure end load P and for $\ell/h \geqslant 1$, the phase angle ψ increases slightly with increasing values of h/H [Fig. 13(a)], while for pure end moment M and $\ell/h \geqslant 1$, the phase angle decreases with increasing values of h/H. The value of the normalised energy release rate G_I/G_I^∞ due to pure end load P decreases significantly, while that due to pure end moment M increases with increasing values of h/H. For example, for $\alpha = 0.5$, $\beta = \alpha/4$ and $\ell/h = 10$, the value of G_I/G_I^∞ due to a pure end load P decreases by 80%, while that due to a pure end moment M increases by 10%, as h/H is increased from 0.1 to 0.33.

The effect of the film/substrate thickness ratio h/H upon the normalised T-stress in the film is shown in Fig. 13(c) for a pure end load P, and is shown in Fig. 13(d) for a pure end moment M, for $\alpha = 0.5$ and $\beta = \alpha/4$. For all values of h/H considered, the normalised T-stress in the film due to P is negative, while that due to M is positive, for all values of ℓ/h in the range $0.1 \leqslant \ell/h \leqslant 20$. The absolute value of T_1h/P for $\ell/h \geqslant 1$ increases slightly with increasing values of h/H [Fig. 13(c)]. The effect of h/H on the T-stress due to a pure end moment M is small [see Fig. 13(d)].

6. CRACK PATH SELECTION MAP

The various criteria for the selection of crack paths discussed in the previous sections can be summarised in the form of a crack path selection map, which also serves as a design guide. The three possible paths for growth of an interfacial crack between a thin film and a substrate are:

(i) continued growth along the interface;

(ii) kinking into the film;
(iii) kinking into the substrate.

Interfacial crack growth occurs if the interfacial toughness is much smaller than the toughness of the adjacent materials and if the interfacial crack tip is open. Kinking into the substrate (or into the film) occurs if the energy condition (8) is satisfied and a mode I path exists in the substrate (or in the film). Recall that a mode I path exists in the substrate if the interfacial phase angle $\psi > \psi_c$, and in the film if $\psi < \psi_c$, where $\psi = \psi_c$ is the phase angle at which a mode I path exists tangentially to the interface. The growth of a kinked crack into the substrate (or into the film) is directionally unstable if the T-stress at the interfacial crack tip is positive and directionally stable if the T-stress is negative; a negative T-stress may also cause a kinked crack to arrest.

A range of expected behaviours is shown in the crack path selection maps of Fig. 14. We take M/Ph and ℓ/h as axes and representative values for (α, β), s/h and h/H. Recall that no growth is predicted if $\mathrm{Re}(Kh^{ie}) < 0$ for the interfacial crack. A mode I kink path exists in the substrate if $\psi > \psi_c$ and a mode I path exists in the film if $\psi < \psi_c$. It is emphasised that kinking will occur only if sufficient energy exists to drive the kink [i.e. if eqn (8) is satisfied]. The kink is directionally stable if $\eta < 0$, and is directionally unstable if $\eta > 0$. Thus, the following crack paths are predicted:

(a) no interfacial crack growth ($\mathrm{Re}(Kh^{ie}) < 0$);
(b) directionally stable kinking into the substrate ($\psi > \psi_c$ and $\eta < 0$);
(c) directionally unstable kinking into the substrate ($\psi > \psi_c$ and $\eta > 0$);
(d) directionally stable kinking into the film ($\psi < \psi_c$ and $\eta < 0$);
(e) directionally unstable kinking into the film ($\psi < \psi_c$ and $\eta > 0$).

These regimes of behaviour are shown in Fig. 14(a) for $\alpha = -0.5$, in Fig. 14(b) for $\alpha = 0$, and in Fig. 14(c) for $\alpha = 0.5$; in each case β is taken to equal $\alpha/4$. There is some rearrangement of the relative dominance of the regimes of behaviour; the $\eta = 0$ line moves down while the $\psi = \psi_c$ line moves up with increasing α. In all cases, no interfacial crack growth is predicted for all ℓ/h provided $M/Ph < -0.2$, and directionally unstable kinking into the film is predicted for $M/Ph > 1$.

7. CASE STUDY

Thouless *et al.* (1987) have investigated the cracking and spalling processes that accompany the edge loading of PMMA and glass plates. A precrack was introduced at the edge of the plate at a depth h from the free surface; the initial length of the precrack $\ell \approx h$. The plate was subjected to various values of the loading parameter M/Ph. Initial growth of the edge crack was found to be unstable under fixed loading. (This is consistent with the results plotted in Fig. 8.) In addition, the initial kinking behaviour of the edge crack depended upon the value of the loading parameter M/Ph.

Since the plate is homogeneous, α and β vanish. We shall compare the predictions of the present study with the experimental observations of Thouless *et al.* (1987). Consider two of the loading parameters reported by Thouless *et al.* (1987); $M/Ph = 0.16$ and $M/Ph = 0.35$. First, take the case $M/Ph = 0.16$. From Fig. 12, we find that $M/Ph = 0.16$ is less than $(M/Ph)_c$ for all values of $\ell/h > 0.1$; kinking into the substrate is therefore predicted subject to the energy condition of eqn (8). For $\alpha = \beta = 0$ we have $\Gamma_I = \Gamma_S = \Gamma_f$. Kinking into the substrate occurs when $G_I/G_S^{max} \leqslant 1$ [eqn (8)]; this condition is satisfied for all values of ℓ/h by the following argument. The curve of G_I/G_S^{max} for $\alpha = \beta = 0$ indicates that $G_I/G_S^{max} \leqslant 1$ for all values of the phase angle $\psi \geqslant -40°$ (He *et al.*, 1991). The results plotted in Figs 8(a) and 8(c) show that ψ is positive for all values of ℓ/h when $M/Ph = 0.16$. We conclude that the energy condition (8) is satisfied for kinking of the crack into the substrate, for all values of ℓ/h. Note that a divergent crack path away from the original crack orientation depends upon the normalised T-stress η being positive. The crack path selection map of Fig. 14(b) shows that the original crack path is directionally stable for $M/Ph = 0.16$ and $\ell/h = 1$. As the crack length increases under a constant value of M/Ph, the mode of

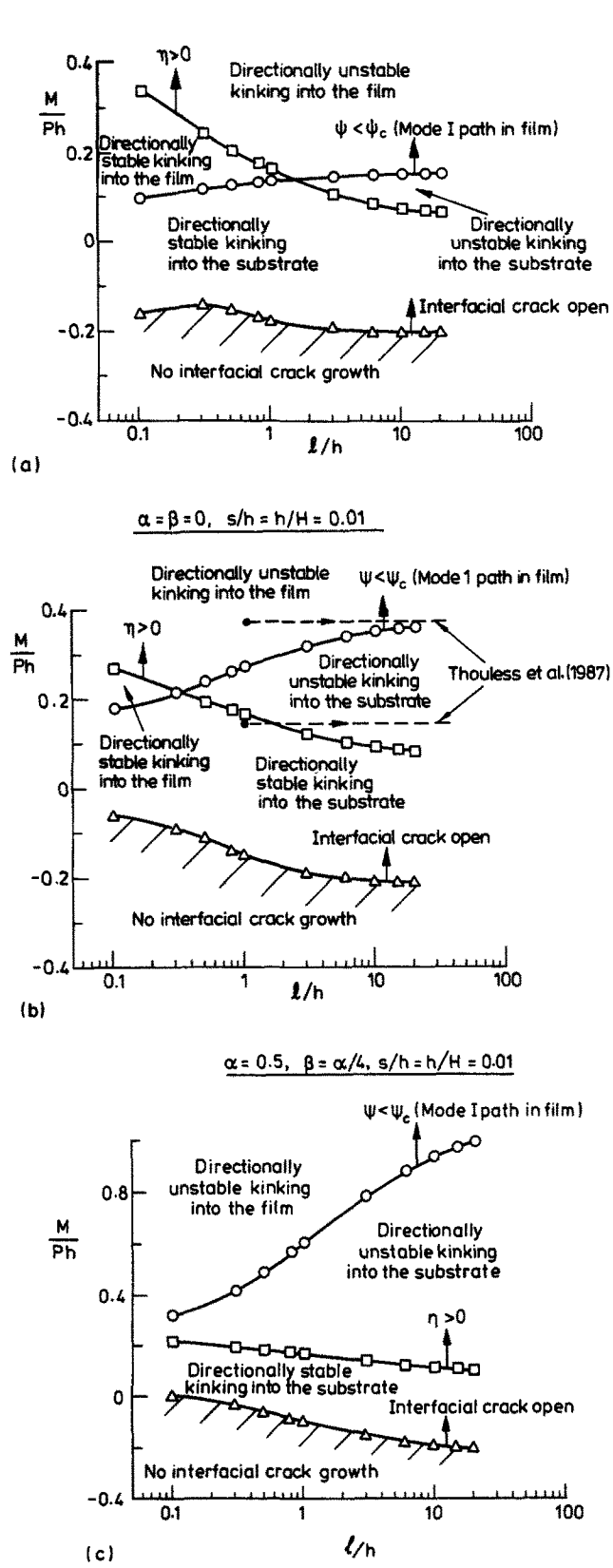

Fig. 14. Crack path selection map in the M/Ph versus ℓ/h plane for a film/substrate thickness ratio $h/H = 0.01$ and an assumed relative interfacial flaw length $s/h = 0.01$: (a) $\alpha = -0.5$, $\beta = \alpha/4$; (b) $\alpha = \beta = 0$; (c) $\alpha = 0.5$, $\beta = \alpha/4$.

failure changes from directionally stable crack growth to directionally unstable kinking into the substrate; the transition occurs at $\ell = 1.1h$ [see Fig. 14(b)]. This is reasonably consistent with the observed crack length of $\ell = 1.5h$ at which unstable kinking into the substrate occurs.

For an initial relative crack length of $\ell/h = 1$ and a loading parameter $M/Ph = 0.35$, the results plotted in Fig. 14(b) predict directionally unstable kinking into the film from the onset of crack growth, provided there is enough energy to drive the kink. From the results plotted in Figs 8(a) and 8(c), the phase angle ψ for $M/Ph = 0.35$ increases from a value of $\psi = -14°$ at $\ell/h = 0.1$ to a value of $\psi \approx 1°$ at $\ell/h = 20$, giving $G_1/G_S^{max} \ll 1$ and the energy criterion (8) is satisfied. Thus, directionally unstable kinking into the film is predicted for all values of ℓ/h. This is in agreement with the observed crack path; the crack with an initial length of $\ell = h$ kinked into the film as soon as it began to grow (Thouless *et al.*, 1987).

8. CONCLUDING DISCUSSION

In this paper an analysis has been presented of the edge cracking and kinking behaviour encountered in many thin film/substrate systems. The stress distribution in the film is decomposed into force and moment components, and the interfacial stress intensity factor and the non-singular crack tip T-stresses are evaluated.

An interfacial crack may continue to grow along the interface or kink into either of the adjoining materials. Kinking of the interfacial crack depends upon satisfaction of the energy condition stated in eqn (8) and upon the existence of a mode I path in the material containing the kink. For given values of material parameters α and β, a critical value of the loading parameter M/Ph exists below which a mode I path ($K_{II} = 0$, $K_I > 0$) exists in the substrate and kinking into the substrate may occur (assuming the substrate is sufficiently brittle). Conversely, kinking into the film may occur (assuming there is sufficient energy to drive the kink) if the loading parameter M/Ph is greater than the critical value. The critical value of the loading parameter $(M/Ph)_c$ is shown in Fig. 12.

The energy release rate for the interfacial edge crack increases with crack extension; the crack is unstable under a fixed load. This contrasts with the case of a debond which initiates from a through-cut in the film; then the interfacial energy release rate decreases with increasing crack length ℓ/h resulting in a stable interfacial crack growth (Beuth, 1992; Akisanya, 1992).

Acknowledgements—The authors are grateful for helpful discussions with Prof. M. F. Ashby and Prof. J. W. Hutchinson, and for financial support from the U.S. Office of Naval Research (Contract Number N00014-91-J-1916).

REFERENCES

Akisanya, A. R. (1992). Interfacial Fracture. PhD Thesis, Cambridge University, U.K.
Akisanya, A. R. and Fleck, N. A. (1992). Brittle fracture of adhesive joints. *Int. J. Fract.* **58,** 93–114.
Akisanya, A. R. and Fleck, N. A. (1993). The decohesion of thin films on brittle substrates. Cambridge University Engineering Department Report, CUED/C-MATS/TR.
Beuth, J. L., Jr (1992). Cracking of thin bonded films in residual tension. *Int. J. Solids Structures* **29,** 1657–1675.
Cao, H. C. and Evans, A. G. (1989). An experimental study of the fracture resistance of bimaterial interfaces. *Mech. Mater.* **7,** 295–304.
Cotterell, B. and Rice, J. R. (1980). Slightly curved or kinked cracks. *Int. J. Fract.* **16,** 155–169.
Dundurs, J. (1969). *Mathematical Theory of Dislocations.* American Society of Mechanical Engineers, New York.
He, M. Y. and Hutchinson, J. W. (1989). Kinking of a crack out of an interface. *J. Appl. Mech.* **56,** 270–278.
He, M. Y., Bartlett, A., Evans, A. G. and Hutchinson, J. W. (1991). Kinking of a crack out of an interface: role of in-plane stress. *J. Am. Ceram. Soc.* **74,** 767–771.
Hu, M. S., Thouless, M. D. and Evans, A. G. (1988). The decohesion of thin films from brittle substrates. *Acta Metall.* **36,** 1301–1307.
Hutchinson, J. W. and Suo, Z. (1992). Mixed mode cracking in layered materials. *Adv. Appl. Mech.* **29,** 63–191.
Kfouri, A. P. (1986). Some evaluation of the elastic T-term using Eshelby's method. *Int. J. Fract.* **30,** 301–315.
MARC-CDC (1974). MARC Research Corporation, Providence, R.I.
Matos, P. P. L., McMeeking, R. M., Charalambides, P. G. and Drory, M. D. (1989). A method for calculating stress intensities in bimaterial fracture. *Int. J. Fract.* **40,** 235–254.
Parks, D. M. (1974). A stiffness derivative finite element technique for determination of crack tip stress intensity factors. *Int. J. Fract.* **10,** 487–501.

Rice, J. R. (1968). A path independent integral and approximate analysis of strain concentration by notches and cracks. *J. Appl. Mech.* **35,** 379–386.
Rice, J. R. (1988). Elastic fracture mechanics concepts for interfacial cracks. *J. Appl. Mech.* **55,** 98–103.
Rice, J. R., Suo, Z. and Wang, J. S. (1989). Mechanics and thermodynamics of brittle interfacial failure in bimaterial systems. In *Metal–Ceramic Interfaces* (Edited by M. Ruhle, A. G. Evans, M. F. Ashby and J. P. Hirth), Vol. 4, pp. 269–294.
Suga, T., Elssner, G. and Schmauder, S. (1988). Composite parameters and mechanical compatibility of material joints. *J. Comp. Mater.* **22,** 917–935.
Suo, Z. and Hutchinson, J. W. (1990). Interface crack between two elastic layers. *Int. J. Fract.* **43,** 1–18.
Thouless, M. D., Evans, A. G., Ashby, M. F. and Hutchinson, J. W. (1987). The edge cracking and spalling of brittle plates. *Acta Metall.* **35,** 1333–1341.
Timoshenko, S. P. and Goodier, J. N. (1970). *Theory of Elasticity*, 3rd edition. McGraw-Hill, New York.

APPENDIX

INTERACTION ENERGY METHOD FOR THE EVALUATION OF THE INTERFACIAL STRESS INTENSITY FACTOR AND THE *T*-STRESSES

In this Appendix we describe the method used to evaluate the interfacial stress intensity factor K and the T-stresses T_1 and T_2 for the thin film/substrate geometry shown in Fig. 2.

Consider a bimaterial specimen containing a traction-free interfacial crack, subjected to a generalised remote load F, as shown in Fig. A1. We assume that plane strain conditions apply. For the interfacial crack shown in Fig. 2(c), the remote loads P and M are represented by the generalised load F. Let (x, y) and (r, θ) be rectangular and polar co-ordinates centred at the crack tip, respectively. We describe below a procedure to evaluate the interfacial stress intensity factor K and the T-stresses due to the load F. The procedure follows from the work of Matos *et al.* (1989) and Kfouri (1986).

The stress field around the crack tip in material m ($m = 1, 2$) due to a remote load F is of the form

$$\sigma_{jk}^m = \frac{Kr^{i\varepsilon}}{\sqrt{2\pi r}} g_{jk}^m(\theta, \varepsilon) + T_m \delta_{1j}\delta_{1k} + O(\sqrt{r}) \qquad j, k = 1,2, \tag{A1}$$

where $K = K_1 + iK_2$ ($i = \sqrt{-1}$) is the complex interfacial stress intensity factor due to F, $g_{jk}(\theta, \varepsilon)$ is a non-dimensional function of angle θ and of oscillatory index ε, T_m is the T-stress in material number m, and δ_{jk} is the Kronecker delta symbol. The full form of the non-dimensional function g_{jk} is listed, for example, by Rice *et al.* (1989). Let the strain and the displacement fields due to F in material m be ε_{jk}^m and u_j^m, respectively.

The path-independent J integral for the elastic body is defined by (Rice, 1968)

$$J = G_1 = \int_C \left(\frac{1}{2}\sigma_{jk}\varepsilon_{jk} n_1 - \sigma_{jk} \frac{\partial u_j}{\partial x} n_k \right) ds, \tag{A2}$$

where C is any contour from the bottom crack surface to the top surface (see Fig. A1), n_j is the outward normal to C, and G_1 is the interfacial energy release rate. Denote the value of J due to the remote load F by $J(F)$.

Consider next an auxiliary field $(\sigma_{jk}^*, \varepsilon_{jk}^*, u_j^*)$ for the same geometry due to a remote load F^*. Let the value of J associated with the auxiliary field be $J(F^*)$. When the displacement fields u_j and u_j^* are summed (and the associated strain fields and stress fields are summed), the value of J for the resulting field $J(F, F^*)$ is given by

$$J(F, F^*) = J(F) + J(F^*) + J_{\text{int}}, \tag{A3}$$

where J_{int} is the interaction integral between the two fields and is given by

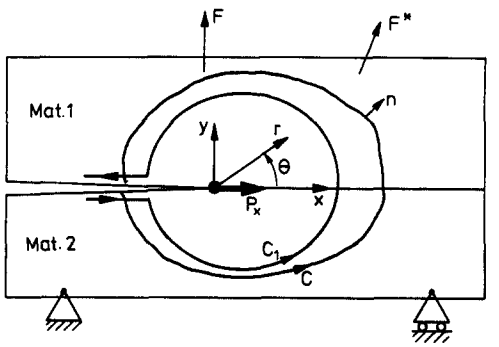

Fig. A1. A cracked bimaterial solid subjected to a generalised external load F. The curves C and C_1 are arbitrary contours starting from the lower crack surface to the top surface.

$$J_{\text{int}} = \int_C \left(\sigma_{jk}\varepsilon^*_{jk} n_1 - \sigma^*_{jk} n_j \frac{\partial u_k}{\partial x} - \sigma_{jk} n_j \frac{\partial u^*_k}{\partial x} \right) \mathrm{d}s. \tag{A4}$$

By suitable choice of the auxiliary field, the integral J_{int} can be expressed in terms of either the interfacial stress intensity factor or the T-stresses, as discussed below.

Evaluation of the interfacial stress intensity factor

Consider as the auxiliary field the singular crack tip field for an interfacial crack. Let the components of the interfacial stress intensity factor associated with this auxiliary field be denoted by K_1 and K_2. We are interested in evaluating the components K_1^* and K_2^* of the interfacial stress intensity factor due to the representative remote load F. From eqns (5) and (A3), superposition of the two fields gives

$$J_{\text{int}} = \frac{2}{E^*}(K_1 K_1^* + K_2 K_2^*). \tag{A5}$$

Here $E^* \equiv (1+\alpha)/(1-\beta_2)\bar{E}_2$ is a function of the elastic properties of the materials. It is evident from eqn (A5) that the value of J_{int} (evaluated by contour integration) can be used to determine the stress intensity factor for the loading state F, by choosing the auxiliary $(\ )^*$ field to be a K_1 field and then a K_2 field in turn.

In order to compute K_1 and K_2, first solve the elastic problem for the remote loading F using the finite element method and obtain $J = J(F)$ via eqn (A2), using Parks' (1974) virtual crack extension method. Then obtain the nodal displacements $\{\Delta u_j\}$ for a problem with the same geometry and for which K_1^* is finite and $K_2^* = 0$. This set of displacements is needed only for the distorted ring of elements during virtual crack extension, and is taken as the asymptotic crack tip displacements for an interfacial crack; the details of the field are listed in Matos *et al.* (1989). Add $\{\Delta u_j\}$ to the finite element displacement solution $\{u_j\}$ for the elastic state of interest, and evaluate $J = J(F, F^*)$ of the resulting field. The difference between $J(F, F^*)$ and the initial $J(F)$ is

$$\Delta J_1 = J(F, F^*) - J(F) = J(F^*) + J_{\text{int}} = \frac{1}{E^*}[(K_1^*)^2 + 2K_1 K_1^*] \tag{A6}$$

and thus

$$K_1 = \frac{E^*}{2}\frac{\Delta J_1}{K_1^*} - \frac{K_1^*}{2}. \tag{A7}$$

The process is repeated by adding to the finite element solution $\{u_j\}$ the asymptotic interfacial crack tip displacements for which $K_1^* = 0$ and K_2^* is finite, to obtain

$$K_2 = \frac{E^*}{2}\frac{\Delta J_2}{K_2^*} - \frac{K_2^*}{2}. \tag{A8}$$

The advantage of this method is its widespread applicability; it can be used for problems with complex loadings and complex crack geometries.

Evaluation of the T-stresses

For evaluation of the T-stress, we choose as the auxiliary field the crack tip field due to a point force in a direction parallel to the interface and located at the crack tip. Consider a point force P_x (per unit thickness) parallel to the crack surface and applied to the interfacial crack tip of the same geometry (shown by the arrow in Fig. A1). When both materials 1 and 2 are semi-infinite in extent, the stresses in both materials due to the point force P_x at the crack tip are given by

$$(\sigma^*_{rr})_1 = -(1+\alpha)\frac{P_x}{\pi r}\cos\theta, \qquad (\sigma^*_{\theta\theta})_1 = (\sigma^*_{r\theta})_1 = 0 \tag{A9}$$

$$(\sigma^*_{rr})_2 = -(1-\alpha)\frac{P_x}{\pi r}\cos\theta, \qquad (\sigma^*_{\theta\theta})_2 = (\sigma^*_{r\theta})_2 = 0 \tag{A10}$$

and the associated displacements are

$$(u_r^*)_1 = (1+\alpha)\frac{P_x}{\pi \bar{E}_1}\left[-\ln\left(\frac{r}{d}\right)\cos\theta - \frac{\theta\sin\theta}{2(1+\nu_1)} \right] \tag{A11}$$

$$(u_r^*)_2 = (1-\alpha)\frac{P_x}{\pi \bar{E}_2}\left[-\ln\left(\frac{r}{d}\right)\cos\theta - \frac{\theta\sin\theta}{2(1+\nu_2)} \right] \tag{A12}$$

$$(u_\theta^*)_1 = (1+\alpha)\frac{P_x}{\pi \bar{E}_1}\left\{ \left[\frac{1+2\nu_1}{2(1+\nu_1)} + \ln\left(\frac{r}{d}\right) \right]\sin\theta - \frac{\theta\cos\theta}{2(1+\nu_1)} \right\} \tag{A13}$$

$$(u_\theta^*)_2 = (1-\alpha)\frac{P_x}{\pi E_2}\left\{\left[\frac{1+2v_2}{2(1+v_2)}+\ln\left(\frac{r}{d}\right)\right]\sin\theta-\frac{\theta\cos\theta}{2(1+v_2)}\right\}, \tag{A14}$$

where the subscripts 1 and 2 denote the material number, d is an arbitrary normalising distance, and E and v are the Young's modulus and the Poisson's ratio, respectively. We note that the stress and displacement fields due to a point force P_x at the tip of a semi-infinite interfacial crack are independent of the material parameter β. When $\alpha = \beta = 0$, the stresses and the displacements due to P_x, given by eqns (A9)–(A14), reduce to the familiar Boussinesq solution [see, for example, Timoshenko and Goodier (1970)].

The auxiliary field due to the point force P_x at the crack tip is added to the near tip field due to F. The J integral $J(F, P_x)$ of the resulting field is obtained by evaluation of eqn (A2) over a circular boundary C_1 centred at the crack tip (see Fig. A1), giving

$$J(F, P_x) = J(F)+J(P_x)+\varepsilon_{xx}P_x+\frac{2}{E^*}(K_1K_1^*+K_2K_2^*). \tag{A15}$$

Here K_1 and K_2 are the components of the complex interfacial stress intensity factor K due to F, which have already been determined by the method described above; K_1^* and K_2^* are the components of the interfacial stress intensity factor due to P_x, and $J(P_x)$ is the value of J when only the point force P_x is applied at the crack tip of the geometry. The strain ε_{xx} is given by

$$\varepsilon_{xx} = \frac{1-v_1^2}{E_1}T_1 = \frac{1-v_2^2}{E_2}T_2. \tag{A16}$$

The fields given by eqns (A9)–(A14) correspond to a strain energy density singularity of the type r^{-2}. Hence $J(P_x) = 0$ and the interfacial stress intensity factor due to P_x vanishes. Thus, eqn (A15) reduces to

$$J(F, P_x) = J(F)+\varepsilon_{xx}P_x. \tag{A17}$$

We implement the above method for estimating the T-stresses T_1 and T_2 for the finite body as follows. First, the J integral $J(F)$ and the interfacial stress intensity factor K due to F are determined using the method of Matos *et al.* (1989). Using the field due to a point force P_x (= 1) at the tip of an interfacial crack between two semi-infinite solids [eqns (A9)–(A14)], the displacements are evaluated at all nodes within a ring of elements surrounding the crack tip. The nodal positions of this ring of elements are deformed during virtual crack extension. The J integral $J(P_x)$ and K_1^* and K_2^* due to P_x (= 1) are then evaluated. The displacements due to F are added to those due to P_x at the nodes of the elements to be deformed, and the J integral of the resulting field $J(F, P_x)$ is evaluated by Parks' virtual crack extension method (Parks, 1974). The evaluated values of $J(P_x)$, K_1^* and K_2^* (all due to P_x) do not vanish due to numerical discretization of the integrals. Thus, we substitute the evaluated values of $J(P_x)$, K_1^* and K_2^* into eqns (A15) and (A16) in order to evaluate T_1 and T_2.